

The survival of interstellar clouds against Kelvin–Helmholtz instabilities

Mario Vietri¹, Andrea Ferrara², and Francesco Miniati³

¹Osservatorio Astronomico di Roma

00040 Monte Porzio Catone (Roma), Italy

E-mail: vietri@coma.mporzio.astro.it

²Osservatorio Astrofisico di Arcetri

50125 Firenze, Italy

E-mail: ferrara@arcetri.astro.it

³Dipartimento di Astronomia, Università di Firenze,

50125 Firenze, Italy

E-mail: miniati@arcetri.astro.it

ABSTRACT

We consider the stability of clouds surrounded by a hotter confining medium with respect to which they are in motion, against Kelvin–Helmholtz instabilities (KHI). In the presence of cooling, sound waves are damped by dissipation. Whenever cooling times are shorter than sound crossing times, as they are in the normal interstellar medium, this implies that the instability generated at the interface of the two media cannot propagate far from the interface itself. To study how this influences the overall stability, first we derive an analytic dispersion relation for cooling media, separated by a shear layer. The inclusion of dissipation does not heal the instability, but it is shown that only a small volume around the interface is affected, the perturbation decaying exponentially with distance from the surface; this is confirmed by numerical simulations. Numerical simulations of spherical clouds moving in a surrounding intercloud medium by which are pressure confined show that these clouds develop a core/halo structure, with a turbulent halo, and a core in laminar flow nearly unscathed by the KHI. The related and previously reported “champagne effect”, whereby clouds seem to explode from their top sides, is cured by the inclusion of radiative losses.

Subject headings: Hydrodynamics – stars: formation

1. Introduction

Shearing flows are ubiquitous in astrophysics. A partial list includes Herbig–Haro objects (Stone, Xu & Mandy 1995), disk plus hot corona accretion flows around compact objects (Liang & Price 1977), wind outflows from galaxies (Wang 1995), jets of all sorts and scales, bipolar flows, and even winds from the progenitor of SN 1987a (Mc Cray & Lin 1994). Besides these, there is the immense class of two–phase media, like the ISM (Spitzer 1978), High Velocity Clouds (Ferrara & Field 1994, Wolfire *et al.*1995), Broad Line Regions of AGNs, protogalaxies (Silk & Norman 1981), Ly α clouds (Sargent *et al.*1980, Giallongo 1995), which are required to give origin to just about everything astrophysical, from stars (Shu, Adams, & Lizano 1987), through Globular Clusters (Vietri & Pesce 1995), to whole galaxies (Ikeuchi & Norman 1991).

Two-phase equilibria are common because they arise through a universal mechanism, thermal instability of radiative media (Field 1965, Balbus 1986), but, equally universally, they are subject to the shearing instability discovered by Kelvin and Helmholtz (KHI from now on), whose potential danger to ISM clouds was noticed in computer simulations at least twenty years ago (Woodward 1976) and is discussed in textbooks (Spitzer 1978).

Possible stabilization of the KHI by magnetic effects was discussed at least as early as 1955 (Michael 1955, Chandrasekhar 1961) and more recently studied in detail by Miura (1984) and, particularly, by Malagoli, Bodo and Rosner (1996). There can be little doubt that this stabilization mechanism is relevant to a large class of phenomena, including jets from AGNs and Galactic sources, and Giant Molecular Clouds. Yet, the magnetic fields in several important astrophysical situations, like Ly α clouds or protogalaxies, may not yet have had the time to grow to values necessary for stabilization, while in other astrophysical situations the role played by the magnetic field is not well-established. It thus seems worth its while to consider idealized situations where magnetic fields are altogether neglected.

The severity of the KHI has been put into sharp focus by numerical simulations of shearing flows around unmagnetized clouds (Murray, White, Blondin and Lin 1993, MWBL from now on) which show that, in the absence of gravity, such clouds are disrupted on a time scale comparable to the flow crossing time of the cloud. These authors considered a dense cloud moving inside a potential well which also contains a tenuous, warm phase, such that the two are in pressure equilibrium. The external gravitational field makes that the cloud speed V be comparable to the warm phase sound speed c_s , so that the relative motion is at the boundary between subsonic and supersonic, $M \approx 1$. Then the cloud is subject to the KHI in a regime close to the incompressible one, where the growth rate is known and large. Especially destructive, in these simulations, was the development of the KHI on the largest scales. The physical explanation for this quick destruction (Doroshkevich and Zel'dovich 1981, DZ, from now on, Nittman, Falle & Gaskell 1982, and Nulsen 1986) is the following: when the cloud is initially placed in a wind, a stagnation point forms ahead of the cloud, whose high pressure accelerates the wind around the cloud; by Bernoulli's theorem, the pressure of the wind is least where its speed is highest, *i.e.*, at the top of the cloud. This pressure minimum is overcome by the inner pressure of the cloud, which is being compressed in the direction of motion by the combined effect of the stagnation point and of its own inertia, and causes an overspilling of the cloud from its top. We shall refer to this as the *champagne effect*.

MWBL and DZ considered the possibility that these clouds were stabilized by self-gravity, showing that this requires a minimum mass M_{min} which, compared to the cloud's Jeans mass M_J is

$$\frac{M_J}{M_{min}} = 0.15 \left(\frac{c_s}{V} \right)^3 \approx 0.1 \quad (1)$$

(MWBL), independent of the density contrast $D \equiv \rho_{warm}/\rho_{cloud}$. Hence a cloud can only choose its own death: by self-gravitational collapse, if $M \gtrsim M_J$, or by disruption by KHI if $M \lesssim M_J$. We shall refer to this result as the *Zel'dovich paradox*.

Is there an alternative to curing the champagne effect, without incurring the Zel'dovich paradox? MWBL and DZ considered an adiabatic fluid; let us drop this assumption, and consider a fluid subject to radiative losses. It is well known that pressure waves in such a fluid are damped more often than amplified as they trudge along (Field 1965, Balbus 1986). This suggests the following remedy: that clouds are (much) larger than the distance over which pressure waves are damped. In this way, when depressurization is occurring at the top faces of the cloud, the inner part will be slow or unable to respond to the matter outflow, and the champagne effect may be slowed down, or possibly altogether removed.

That cooling times are shorter than cloud crossing times may run counter to intuition (Malagoli, Bodo and Rosner 1996), but this certainly applies to the local ISM, where typical cooling times are $\approx 10^4 \text{ yr}$ and sound speeds $\approx 1 \text{ km s}^{-1}$ (Spitzer 1978), resulting in damping lengths of $\approx 3 \times 10^{16} \text{ cm}$, much smaller than typical cloud radii. Thus pressure waves carrying the Kelvin–Helmholtz instability inside the cloud are damped before crossing the whole cloud.

We are thus trying to stabilize the KHI in a local sense. We do not expect to find a dispersion relation for the Kelvin–Helmholtz modes which shows them to be stable. Rather, we expect to find a situation where the KHI is always present, except that it is *unable to propagate far from the interface*, and thus entrain in a catastrophic fate the whole cloud.

The flow of the argument and the plan of the paper are as follows: in the next Section, we derive analytically the dispersion relation for the shear layer between two idealized, radiative fluids. This problem is then tackled numerically in Sec. 3, and it is shown that the KHI is not healed, but that it is confined to a narrow region around the surface of discontinuity. In Section 4, we present numerical simulations of a realistic cloud embedded in a light wind with Mach number ≈ 1 , for both the adiabatic and the radiative cases. It is shown here that the inclusion of radiative effects cures the champagne effect. This section also contains the simulation of a cloud for a duration far exceeding the expected KHI timescale, in an effort to show that the core/halo structure that radiative clouds develop to withstand the KHI is statistically time-independent, and stable. A brief discussion in Section 5, and a short summary in Section 6 close the paper.

2. The dispersion relation

We want to derive the dispersion relation for the Kelvin–Helmholtz instability for two inviscid, but compressible and radiative fluids separated by a tangential discontinuity, located at the $z = 0$ plane in the unperturbed problem. The zero-th order situation that we envision thus has an upper fluid occupying the $z > 0$ semispace, and moving rightward with speed $v = V > 0$, while the lower one occupies the lower ($z < 0$) semispace, and is moving leftward with speed $v = -V < 0$. The two fluids are both supposed to be in thermal and pressure equilibrium. Since the point we wish to make is rather general, we consider an idealized fluid whereby radiative losses balance radiative gains (per unit volume) $\Lambda = 0$, where the idealized forms of the net cooling function we choose is

$$\Lambda = \rho^2 L(T)/m_H - \dot{E}\rho \tag{2}$$

with m_H is the mass per particle, and we neglect chemical composition effects. It is understood that both $L(T)$ and \dot{E} can be different for the two fluids. The two fluids are in pressure equilibrium with each other, which entails $\rho_+ c_{s,+}^2 = \rho_- c_{s,-}^2$, where c_s is the sound speed, and we distinguish the upward, rightward moving fluid with a + subscript, and the lower, leftward moving fluid with a – subscript. Lastly, we shall also impose that each fluid is stable with respect to the Field (1965) instability, which can be obtained by imposing

$$\frac{d \ln L(T)}{d \ln T} \equiv q > 1 . \tag{3}$$

The reason why we introduce a heating, albeit idealized, and the parameter q is to make sure that no local instability affects our analysis, and that any further instability we may find is simply due to the instability of the tangential discontinuity.

Next we wish to perturb the equations of fluid dynamics pertaining to each fluid separately; thus we supplement the usual equations

$$\frac{\partial \rho}{\partial t} + \nabla \cdot (\rho \vec{v}) = 0 \quad (4)$$

$$\frac{\partial \vec{v}}{\partial t} + \vec{v} \cdot \nabla \vec{v} = -\frac{\nabla p}{\rho} \quad (5)$$

with the energy equation appropriate to a nonviscous, but radiative fluid

$$\frac{3}{2} \rho \left(\frac{\partial}{\partial t} + \vec{v} \cdot \nabla \right) T - T \left(\frac{\partial}{\partial t} + \vec{v} \cdot \nabla \right) \rho = \Lambda. \quad (6)$$

We now consider perturbations of the form

$$\delta X \propto e^{nt} e^{ik_x x} e^{ik_y y} f(z) \quad (7)$$

where the still unspecified z -dependence derives from the fact that the zero-th order problem is not homogeneous in the z -direction. We shall also use, for the convective derivative, the notation

$$N \equiv n + ik \cdot \vec{V} \quad (8)$$

for the same reason. Perturbing and linearizing the hydrodynamic equations in either fluid we find

$$N \delta \rho + \rho \nabla \cdot \delta \vec{v} = 0 \quad (9)$$

$$N \delta \vec{v} = -\frac{\nabla \delta p}{\rho} \quad (10)$$

$$\frac{3}{2} N \rho \delta T - T N \delta \rho = -(\Lambda_\rho \delta \rho + \Lambda_T \delta T) \quad (11)$$

where we have used

$$\Lambda_\rho \equiv \frac{\partial \Lambda}{\partial \rho}, \quad \Lambda_T \equiv \frac{\partial \Lambda}{\partial T}. \quad (12)$$

We now determine the z -dependence of our problem. By straightforward computations we eliminate δT between Eq.11 and the equation of state $p = \rho T / m_H$, (Boltzmann's constant k_B is included in the definition of T , which is thus an energy) to express δp in terms of $\delta \rho$, next we plug this δp into Eq. 10 and then eliminate $\nabla \cdot \delta \vec{v}$ between Eq. 10 and Eq. 9 to obtain

$$\frac{1}{f} \frac{d^2 f(z)}{dz^2} = k^2 + m_H N^2 \left[T + \rho \frac{TN - \Lambda_\rho}{3\rho N/2 + \Lambda_T} \right]^{-1} \equiv k_a^2. \quad (13)$$

The right hand side of this equation does not depend upon z , thus neither can the right hand one. We thus find for the z -dependence that

$$f = \begin{cases} e^{-k_a z} & \text{if } z > 0 \\ e^{k_a z} & \text{if } z < 0 \end{cases} \quad (14)$$

where we have implicitly assumed $Re(k_a) > 0$.

It is convenient to rewrite k_a somewhat. We have

$$\Lambda_\rho = \frac{\rho L}{m_H}, \quad \Lambda_T = \frac{\rho^2}{m_H} \frac{dL}{dT}, \quad (15)$$

where we used the thermal equilibrium condition that applies to the zero-th order solution, *i.e.* $\Lambda_0 = 0$. Now we also define the net cooling time

$$\tau \equiv \frac{3}{2} \frac{m_H T}{\rho L(T)} \quad (16)$$

and use the sound speed $c_s^2 = 5T/(3m_H)$, to obtain

$$k_a^2 \equiv k^2 + \frac{N^2}{c_s^2} \frac{N\tau + q}{N\tau + 3(q-1)/5} \quad (17)$$

k_a^2 is complex-valued, since it depends upon N , implying that there will always be a k_a such that $Re(k_a) > 0$, and this, in turn implies (Eq. 14) that each perturbation penetrates only a finite amount inside the cloud. This is true also for incompressible fluids, where it can be shown that the damping wavenumber $Re(k_a) \propto k$; in this case, clouds of finite size are always perturbed through their whole volume by KH perturbations of suitably small wavenumbers. Dimensionally, this occurs because there is no other wavenumber in this idealized problem; however, in the problem where cooling losses are included, there is another wavenumber, $1/c\tau$. It will be shown later on, in Section 5, that this changes $Re(k_a)$ in a dramatic way: in fact, we shall find that $Re(k_a) \gtrsim 1/c\tau$ for *every* wavenumber, so that, provided the cloud radius much exceeds $\approx c\tau$, most of the cloud volume cannot be penetrated by the KH perturbations.

Incidentally, this also simplifies the problem at hand, by allowing us to neglect the usual need to determine which solutions for the growth rate belong to solutions with incoming or outgoing waves: once a solution for n has been identified, the corresponding spatial part is the only physical one, *i.e.*, the root of Eq. 17 such that the perturbation decays away from the mid-plane. This argument also shows that any solution of the dispersion relation, to be derived in the following, is physical, *i.e.*, it has a spatial part consistent with the idea that only perturbations emanating from the surface of discontinuity (as opposed to reaching it) ought to be included.

Now that we have determined the z -dependence of our problem, we turn to the dispersion relation that we obtain by assuring that the pressure is continuous across the perturbed interface. We consider a displacement of the $z = 0$ interface by an amount ζ in the z -direction, and we assume for it a dependence

$$\zeta \propto e^{nt} e^{ik_x x} e^{ik_y y} \quad (18)$$

so that the z -velocity of a particle lying at the interface, δv_z , is given by

$$\delta v_z = \left(\frac{\partial}{\partial t} + \vec{V} \cdot \frac{\partial}{\partial \vec{x}} \right) \zeta = N\zeta. \quad (19)$$

On the other hand, from Eq. 10, we find

$$\delta v_z = \pm \frac{k_a \delta p}{N\rho} \quad (20)$$

where we have used Eq. 14, and the upper sign refers to the semispace $z > 0$, the lower one to $z < 0$. Eliminating δv_z from the two equations above, we find

$$\frac{N_+^2 \rho_+}{k_{a,+}} = - \frac{N_-^2 \rho_-}{k_{a,-}} \quad (21)$$

where, as stated above, the subscripts distinguish the fluids above and below the tangential discontinuity. Since $v = V > 0$ for $z > 0$, and $v = -V$ for $z < 0$, we find

$$N_+ = n + i\vec{k} \cdot \vec{V}, \quad N_- = n - i\vec{k} \cdot \vec{V}. \quad (22)$$

We must remember that $k_{a,\pm}$ depends upon N_{\pm} through Eq. 17, and that the thermodynamic properties of the two fluids (ρ, T, c_s, q) may be different. We also define for convenience

$$y \equiv \frac{n}{c_{+,s}k}, \quad D \equiv \frac{\rho_+}{\rho_-}, \quad r_{\pm} \equiv c_{+,s}k\tau_{\pm}, \quad R \equiv \frac{c_{+,s}^2}{c_{-,s}^2} \quad (23)$$

Eq. 21 is the dispersion relation we are seeking. It depends upon cooling and heating processes only through the cooling time τ ; no simple analytic solutions are possible for the general case.

First, we study the solutions of Eq. 21 in the case of identical fluids, *i.e.*, $D = 1$. The real part of y for the growing mode is shown in Fig. 1 for the particular value $q = 1.1$ (the solutions are not very sensitive to q as long as $q > 1$, as required for thermal stability). Deviations from the purely adiabatic case (corresponding to $r \propto \tau \rightarrow \infty$) as r is progressively decreased are clearly seen. For small values of r the curves approach asymptotically the isothermal solution ($r = 0$). Stabilization of the KHI occurs at the critical Mach number $M_c \geq \sqrt{2}$ for an adiabatic fluid, while in presence of radiative losses there are no stable regions, even though the growth rate are noticeably smaller. In the incompressible regime (small Mach numbers) it is $Re(y) \propto M$ independently of r , thus recovering the classical result; however, deviations from linearity occur already at $M \sim 0.3$. In summary, high-Mach number flows are destabilized by inclusion of radiation, and low-Mach number ones tend to be more stable.

Next, we study the influence of the density contrast D on the stability of the fluid. For the *adiabatic* case, in Fig. 2 we show the real part of y for the fastest growing mode, obtained by numerical solution of Eq. 21, as a function of Mach number, and for several values of the density contrast D . The most apparent features are: (i) the critical value M_c decreases with increasing D , thus expanding the stability region well inside the subsonic domain; (ii) the amplitude of the growth rate decreases with increasing D , and the location of its maximum shifts towards lower values of M . Note that for $D = 0.002$, Mach numbers larger than 0.6 are absolutely stable. The situation is considerably modified by the inclusion of radiative losses as shown by Fig. 3, which refers to the parameters $D = 0.002$, $q_+ = q_- = 1.1$, $r_+ = 10^6$. The choice for r_+ is motivated by the fact that one can prove that a background medium with the characteristics of the intercloud medium of the Galaxy can be considered, to the present purposes, as very close to adiabatic ($r_+ \gg 1$). As a general result, we find that cooling processes exacerbate the KHI: the peak of the growth rate located around $M \sim 0.5$ is amplified as the system departs from the adiabatic limit, and all Mach numbers become unstable, even though with moderate growth rates, $Re(y) < 0.1$. Also, two different unstable modes are found, one of which becomes marginally stable ($Re(y) = 0$) in the adiabatic case (compare with Fig. 2).

3. Numerical experiments for the shearing layer

To check and extend the above analytical results we have performed a large number of numerical simulations. To this aim we have used a hydrodynamic code based on a 2D TVD-MUSCL shock-capturing scheme (Van Leer 1979, Jacobs 1991); the code is accurate to second order in both space and time. The total grid in the highest resolution models presented below is 200 by 90 zones. The code has positively passed all the standard hydrodynamical tests.

We have run two different types of experiments simulating a shearing layer and a cloud engulfed by a wind; in the following we describe the shearing layer experiment, leaving the discussion of the simulations

of the cloud in a wind to the next Section.

In the first class of experiments the lower part of the grid is filled with a uniform fluid of density ρ_- and sound speed $c_{-,s}$ moving leftwards at a Mach number $M = V/c_{-,s}$ and the upper part is filled with a uniform fluid of density ρ_+ and sound speed $c_{+,s}$ moving rightwards at the same speed. The density contrast between the two fluids is $D = \rho_+/\rho_- = 2 \times 10^{-3}$ and they are supposed to be in pressure equilibrium (*i.e.*, $D = 1/R$, see Eq. 23). The density at the interface is discontinuous and we assume the gas to evolve *adiabatically*, *i.e.*, $\Lambda = 0$. We have imposed a sinusoidal initial perturbation of the velocity field, with wavelength equal to the grid size and 5% amplitude; the perturbation is centered around the interface on a strip encompassing 9 grid zones.

Fig. 4 shows a snapshot of the density and velocity field for the two values of the shearing Mach number $M = 0.5$ and $M = 0.8$ for the adiabatic case and $D = 2 \times 10^{-3}$, at times $t = 3.6\tau_d$, and $t = 7.3\tau_d$, respectively; $\tau_d = \ell/V D^{1/2}$ is the linear growth time of the instability. For $M = 0.5$ a structure similar to the “Kelvin’s cat’s eyes” of the KHI is clearly recognized, whereas for $M = 0.8$ the initial perturbation is quickly damped leading to a stable state. Hence, the numerical simulations confirm the results obtained analytically: in the adiabatic case (and $D = 2 \times 10^{-3}$) the KHI is stabilized for $M > 0.6$.

Fig. 5 shows a plot of the density and velocity field for the case of two identical fluids, with $M = 0.5$, in the adiabatic and radiative cases for the two panels, respectively. The value of r - the ratio between the cooling time and the sound crossing time - for this simulation is 6×10^{-3} . Here it can be seen that the inclusion of radiation affects the shear layer stability exactly as predicted by the analytic dispersion relation (Fig. 2): for this value of M both panels should be unstable, but the lower one on a much longer time scale. In fact, the results show that in the radiative case at $t > 20\tau_d$ there is no trace of the instability yet, as expected.

4. Numerical experiments for a cloud engulfed by a wind

The same two-dimensional code mentioned in the previous section was used to study the more realistic problem of a cloud moving in a background medium by which it is pressure-confined. An important caveat is needed here: it is well-known (Bayly *et al.*, 1988) that the existence of nonlinear shear instability requires three dimensions, so that a purely two-dimensional simulation is necessarily limited in scope. It is nonetheless useful as a first crack of the problem to check whether the ideas discussed above do produce a stabilization. Further, three-dimensional simulation shall be presented elsewhere.

Since it would be impractical to simulate such a situation, due to the very large grids required to follow the cloud motion, we study instead the related problem of a cloud engulfed by a wind moving at a given Mach number $M = V/c_{+,s}$, where $c_{+,s}$ is the sound speed in the wind. The subtleties related to this different approach are discussed in detail by MWBL, who found that the physics of the KHI is not changed by the possible onset of Rayleigh-Taylor instabilities, which can be shown to grow on a much longer timescale. Some care has to be devoted to the choice of the boundary conditions of the problem. That at the bottom of the grid is *free-slip*, to exploit the symmetry of the problem (to save computational time we consider only half a cloud); the conditions at the other three grid boundaries are selected according to the speed of the flow.

The cloud is supposed to be a factor 500 denser than the background wind, and moving at $M = 0.8$. We have selected this value of M since from the above discussed linear analysis it should correspond to a stable

configuration (as it is indeed for the shearing layer even in the nonlinear regime). In addition, we show the cloud evolution both in the adiabatic (Fig. 6) and in the radiative (Fig. 7) case. The net cooling function adopted is the canonical one (see for details Ferrara & Field 1994) allowing for a two phase cloud-intercloud medium; thus both the cloud and the wind are initially in thermal equilibrium. The physical conditions for the cloud and the wind are $n_- = 1 \text{ cm}^{-3}$, $T_- = 16 \text{ K}$, $\ell \sim 40 \text{ pc}$, and $n_+ = 2 \times 10^{-3} \text{ cm}^{-3}$, $T_+ = 8000 \text{ K}$, respectively; here n_+ is the wind number density, T_+ its the temperature and ℓ is the cloud radius. Using the previous parameters we can derive $r_+ \sim 30$ and $r_- \sim 0.4$. As emphasized already, the wind is much less radiative than the cloud, and this situation, as readily realized from a comparison of Figs. 2 and 3, leads to a stronger KHI with respect to the case in which both fluids are adiabatic. In the simulations, no gravity whatsoever is included.

From an inspection of Fig. 6 we see that the cloud becomes highly flattened with sharp density and pressure gradients along the edges. A vortex sheet develops in the rear part of the cloud initiating a mass loss from the cloud itself. A certain degree of arbitrariness is present when identifying the cloud at each time step and therefore defining the mass loss. For this reason we have plotted (thick line in Fig. 6) the isocontour encompassing 90% of the initial mass. At the last calculated evolutionary time ($t = 4\tau_d$, where $\tau_d = \ell/V D^{1/2}$ is the linear growth time of the instability) the cloud appears to be extremely distorted. The effect which we dubbed 'champagne effect' is patently obvious.

Fig. 7 presents the analogous simulation for the radiative case. The evolution is similar, but the instability appears less pronounced, as can be appreciated from the velocity structure of the vortex. The cloud appears to be more rounded and the density gradients less steep.

The most obvious feature of Fig. 7, when compared with Fig. 6, is that the innermost density contours are much less strongly distorted; actually, the cloud's core does not seem to have expanded at all. This visual impression is borne out by Fig. 8, where we plotted the time evolution of the volumes occupied by the innermost 25%, 50%, 75% and 90% of the mass, for both the adiabatic and the radiative simulations. From these it is apparent that the outermost mass shells expand in both simulations, albeit by different amounts, while the innermost ones behave in a radically different way: they expand for the adiabatic case, and they contract for the radiative one. Hence, the visual impression of disruption that MWBL attributed to their simulations (here effectively reproduced in our Fig. 6) is strongly reduced by inclusion of radiative losses.

The next obvious question is to see whether the stratification of the radiative cloud seen in Fig. 7 is in some sense stable. In Fig. 9 we show the time evolution of a special simulation which we carried out for a rather long time, $t = 7.47\tau_d$. The total time span of this simulation is limited neither by computational power, nor by our patience, but by the fact that, in the adopted reference frame, the cloud falls off the right hand edge because of the net deceleration that the wind imparts to the cloud center of mass. Extension of Fig. 9 to longer timescales requires a prohibitively large computational grid. Still, Fig. 9 manages to convey the obvious feeling that the cloud's modification has by and large stopped at $t \sim 6\tau_d$, and from then on the cloud is essentially in a statistical equilibrium, with a well-developed core/halo structure.

Fig. 9 contains our major result, that sheared clouds are stabilized against the KHI by radiative effects, without any appeal to self-gravity which is here completely neglected.

5. Discussion, with a solution of Zel'dovich paradox

It is well-known that, when the detailed structure of the shear layer is considered, modes with wavelengths shorter than the width of the region over which there is a significant velocity gradient are stabilized against the KHI (Chandrasekhar 1961). Accordingly, Nulsen (1982) has argued that all modes with wavelength smaller than a cloud radius are also stabilized. However, MWBL’s simulations, and Fig. 7 above bear witness to the strength of the remaining instability. We thus concentrate on these, longer wavelength modes, and consider Eq. 17 on the cold, dense side of the interface. Since $kc_{-,s}\tau_- \ll 1$

$$Re(k_a) \approx \frac{N}{c_{-,s}} \left(\frac{N\tau_- + q}{N\tau_- + 3(q-1)/5} \right)^{1/2}. \quad (24)$$

We need to treat separately the two cases $N\tau_- \gg 1$ and $N\tau_- \ll 1$.

5.1. Case 1: $N\tau_- \gg 1$

In this case, we find

$$Re(k_a) \approx \frac{Re(n)}{c_{-,s}} + \frac{2q+3}{10} \frac{1}{c_{-,s}\tau_-}. \quad (25)$$

Here we can take $Re(n) \lesssim kVD^{1/2}$ (D is the density contrast between warm and cold phases, Eq. 23), the value for incompressible fluids, because we know from Fig. 3 that the real instability timescale is longer for the compressible, radiative case. Then it can be shown that the second term dominates the first one if the cloud radius ℓ much exceeds ℓ_{c1} , where

$$\ell_{c1} = \frac{10D^{1/2}}{2q+3} 2\pi V\tau_-. \quad (26)$$

From the condition of pressure balance between the two phases, and that of barely sonic motion, it can be seen that the above condition is equivalent, in order of magnitude, to $kc_{-,s}\tau_- \ll 1$. We then obtain

$$Re(k_a) \approx \frac{2q+3}{10} \frac{1}{c_{-,s}\tau_-}. \quad (27)$$

From the above we find that $Re(k_a) \gg 1$ because of our assumption $kc_{-,s}\tau_- \ll 1$, so that perturbations are damped in this radius range. Thus all clouds with radius in the range

$$2\pi c_{-,s}\tau_- < \ell < 2\pi V\tau_- \quad (28)$$

are stabilized against KHI.

5.2. Case 2: $N\tau_- \ll 1$

The square root in Eq. 24 can now be approximated to yield

$$Re(k_a) \approx \frac{5q}{3(q-1)} \frac{Re(n)}{c_{-,s}} + \frac{25(2q+3)}{9(q-1)^2} \frac{k^2 V^2 \tau_-}{2c_{-,s}}. \quad (29)$$

Again using for $Re(n)$ the value for incompressible fluids, we see that the second term dominates the first one for $\ell \ll \ell_{c2}$, where

$$\ell_{c2} = \frac{2q+3}{6q(q-1)D^{1/2}} 2\pi V \tau_- . \quad (30)$$

In this case, Eq. 29 can be approximated by retaining only the second term, and it can be shown that $Re(k_a) \gg 1$. Again, we find that all modes with radius in the range

$$2\pi V \tau_- < \ell < \frac{2q+3}{6q(q-1)D^{1/2}} 2\pi V \tau_- \quad (31)$$

are stabilized against the KHI. Together, Eq. 28 and 31 imply that all modes in the range

$$2\pi c_{-,s} \tau_- < \ell < \frac{2q+3}{6q(q-1)D^{1/2}} 2\pi V \tau_- \quad (32)$$

are stabilized against the Kelvin–Helmholtz modes. It should be noticed that the above estimate is pessimistic, because, in deriving it, we have used the instability rate for incompressible fluids, rather than the slower one for realistic, compressible and radiative fluids of Fig. 3. For a numerical evaluation, we use the standard ISM parameters (Spitzer 1978): $\tau_- \approx 10^4 \text{ yr}$, $c_{-,s} \approx 1 \text{ km s}^{-1}$, $V \approx 10 \text{ km s}^{-1}$, to obtain that all clouds in the range $0.03 \text{ pc} < \ell < 33 \text{ pc}$ are stabilized. In particular, our simulations use the numerical values $\tau_- = 7 \times 10^5 \text{ yr}$, $c_{-,s} = 0.4 \text{ km s}^{-1}$, $V = 8 \text{ km s}^{-1}$ which implies that the cloud size we have adopted ($\ell = 40 \text{ pc}$) is well into the corresponding range of stability $2 \text{ pc} < \ell < 3000 \text{ pc}$.

We can now discuss the solution of the Zel’dovich paradox. We compare ℓ_{c2} with the Jeans length for a cloud ℓ_J :

$$\frac{\ell_{c2}}{\ell_J} \approx 1 \quad (33)$$

for the standard ISM parameters. This implies that all clouds with mass $10^{-6} M_J < M < M_J$ are stabilized. This ought to be contrasted with Eq. 1.

The above argument shows that clouds are stable, at least for a time comparable to the dynamical time scale τ_d . The larger question of the persistence of this flow, *i.e.*, how long the cloud with the core/halo structure will persist, can be dealt with here only approximately. The persistence clearly depends upon two factors: first, the net rate (gains minus losses) of mass entrainment of the cloud by the hotter medium, which we cannot determine here but which is surely smaller than $\lesssim \pi \ell^2 \rho_h V$, where ρ_h is the density of the warm phase. Second, the kinetic energy losses due to the acceleration (in the cloud system of reference) of the warm phase matter. Both arguments lead to a deceleration timescale τ_d of order

$$\tau_d = \frac{4}{3} \frac{R}{V} \frac{\rho_c}{\rho_h} \approx 300 \frac{R}{V} , \quad (34)$$

which shows the survival time to be a few hundred times the dynamical timescale, $\approx 3 \times 10^8 \text{ yr}$. Most likely, this time is long enough for other factors like collisions to become important. In summary, the inclusion of radiative effects has eliminated the Zel’dovich paradox, leaving a range of ≈ 6 orders of magnitude of mass within which clouds are stable with respect to both self-gravity and KH modes.

Another caveat that is worth discussing is that it is not at all obvious that clouds in the ISM, and the confining gas should be in thermal equilibrium, but this only strengthens our arguments. It seems in fact that most clouds are slowly cooling down, with unreplenished losses. When the equation of state softens as the pressure waves trudge along, they are damped: they put more work into compressing the ISM than is returned to them because of radiative losses. So, by considering a situation of thermal equilibrium, we have

put ourselves into the least favorable conditions. That some kind of stabilization is however achieved under these circumstances seems to us a sufficiently general point worth making.

The last point we wish to make is that the above discussion closely parallels that made in textbooks (Landau and Lifshitz 1987) for the development of the phenomenon of separation in incompressible fluids, whereby turbulent, rotational eddies cannot penetrate the laminar flow region, with a skin depth $\propto k^{-1}$. This is exactly similar to the discussion above, except for the different dependence of the skin depth upon wavenumber. Still, the parallel suggests where, ultimately, the shear energy will go: in turbulence of a thin layer around the surface of separation, without disturbing the laminar flow of the remaining region, a conclusion which we cannot, formally, extrapolate neither from our linear computations, nor from our coarse numerical simulations.

6. Summary

In this paper we have tried to show what follows:

- the KHI is not stabilized by inclusion of radiative losses;
- however, the instability is contained within a small volume around the surface of discontinuity;
- thus stabilization occurs because cooling/heating timescales are shorter than dynamical ones: the instability does not extend much beyond the interface, and thus does not penetrate the main bodies of fluid involved;
- this is borne out by analytical and numerical treatment of the shear layer;
- clouds with radiative losses are stabilized against the ‘champagne effect’;
- this happens through the development of a core/halo structure whereby the halo is turbulent but incapable of exporting this turbulence into the denser core, where laminar flow still prevails;
- this defense mechanism, based only on thermodynamic and hydrodynamic details, ought to be reasonably universal, and apply to the large range of physical conditions covered by two-phase equilibria.

Our major result is visible in Fig. 9, where the evolution of a cloud for a time much longer than the timescale on which the KHI is expected to operate has been followed, showing that the radiative cloud has reached a statistical equilibrium.

Thanks are due to an anonymous referee for comments that greatly improved the manuscript.

REFERENCES

- Balbus, S., 1986, ApJ, 303, 79.
- Bayly, G.B., *et al.*, 1988, Ann. Rev. Fluid Mech., 20, 359.
- Chandrasekhar, S., 1961, Hydrodynamic and hydromagnetic stability, Clarendon Press:Oxford.
- Doroshkevich, A.G., Zel'dovich, Ya.B., 1981, Soviet-Phys.-JETP, 53,405(DZ).
- Ferrara, A., Field, G.B., 1994, 423, 665.
- Field, G.B., 1965, ApJ, 142, 531.
- Giallongo, E., 1995, in ‘The Physics of the Interstellar and Intergalactic Medium’, ed. by A. Ferrara, C.F. McKee, C. Heiles and P.R. Shapiro, ASP Conf. Ser., Vol. 80, 98.
- Ikeuchi, S., Norman, C.A., 1991, ApJ, 375, 479.
- Jacobs, P. A. 1991, Tech. Rep. ICASE, Interim Report 18, ICASE.
- Landau, L.D., Lifshitz, E.M., 1987, Fluid Mechanics, Pergamon Press: Oxford.
- Liang, E.P.T., Price, R.H., 1977, ApJ, 218, 247.
- Malagoli, A., Bodo, G., Rosner, R., 1996, ApJ, 456, 708.
- McCray, R., Lin, D.N.C., 1994, Nature, 369, 378.
- Michael, D.H., 1955, Proc. Camb. Phil. Soc., 51, 528.
- Miura, A. 1984, JGR, 89, 801.
- Murray, S.D., White, S.D.M., Blondin, J.M., Lin, D.N.C., 1993, ApJ, 407, 588 (MWBL).
- Nittman, J., Falle, S.A.E.G., Gaskell, P.H., 1982, MNRAS, 201, 833.
- Nulsen, P.E.J., 1982, MNRAS, 198, 1007.
- Nulsen, P.E.J., 1986, MNRAS, 221, 377.
- Sargent, W. L. W., Young, P. J., Boksenberg, A. & Tytler, D. 1980, ApJS, 42, 41
- Shu, F.H., Adams, F.C., Lizano, S., 1987, ARA&A, 25, 23.
- Silk, J., Norman, C., 1981, ApJ, 247, 59.
- Spitzer, L., 1978, Physical Processes in the Interstellar Medium, Wiley: New York.
- Stone, J.M., Xu, J., Mundy, L.G., 1995, Nature, 377, 315.
- Van Leer, B. 1979, J. Comput. Phys., 32, 101.
- Vietri, M., Pesce, E., 1995, ApJ, 442, 618.
- Wang, B., 1995, ApJ, 444, 590.
- Wolfire, M. G., McKee, C. F., Hollenbach, D. & Tielens, A. G. G. M. 1995, ApJ, 453, 673.
- Woodward, P.R., 1976, ApJ, 207, 484.

Fig. 1.— Nondimensional growth rates $y = n/c_s k$ as a function of the flow Mach number (unstable mode) for the identical fluids ($D = 1$) case with $q = 1.1$. The numbers show the value of the parameter r (the ratio between cooling and sound crossing time of the perturbation) for the radiative cases; the label a denotes the adiabatic case.

Fig. 2.— Nondimensional growth rates $y = n/c_{+,s} k$ as a function of the flow Mach number (unstable mode) for the different, adiabatic fluids case. The numbers show the value of the parameter D , the density contrast between the two fluids.

Fig. 3.— Nondimensional growth rates $y = n/c_{+,s} k$ as a function of the flow Mach number (for the two unstable modes) for the different, radiative fluids case with a density contrast $D = 0.002$, $q_+ = q_- = 1.1$, and $r_+ = 10^6$. The numbers show the value of the parameter r_- for the two unstable modes.

Fig. 4.— Advanced stages of the evolution of the shearing layer with $D = 0.002$. The two cases differ for the fluid Mach number: $M = 0.5$, time $t = 3.6\tau_{d1}$ (upper panel) and $M = 0.8$, $t = 7.3\tau_{d2}$ (lower panel). Due to the different Mach number, the corresponding dynamical times τ_{d1} and τ_{d2} (see Sec. 3) are different. The whole rectangular grid is presented here; logarithmic density levels (contours) and velocity field (arrows) are plotted. Density values range from $n_{min} = .8 \text{ cm}^{-3}$ to $n_{max} = 577.5 \text{ cm}^{-3}$; velocity values range from $v_{min} = .012$ to $v_{max} = .88$ (in units of the isothermal sound speed in the rarefied gas).

Fig. 5.— Advanced stages of the evolution of the shearing layer with $D = 1$ and Mach number $M = 0.5$; the adiabatic (upper panel) and radiative $r \sim 10^{-3}$ (lower panel) cases are shown at times $t = 6.76\tau_d$ and $t = 22.8\tau_d$, respectively. logarithmic density levels (contours) and velocity field (arrows) are plotted. For the adiabatic case density values range from $n_{min} = .77 \text{ cm}^{-3}$ to $n_{max} = 1.05 \text{ cm}^{-3}$; for the radiative case density values range from $n_{min} = 1.0 \text{ cm}^{-3}$ to $n_{max} = 1.02 \text{ cm}^{-3}$.

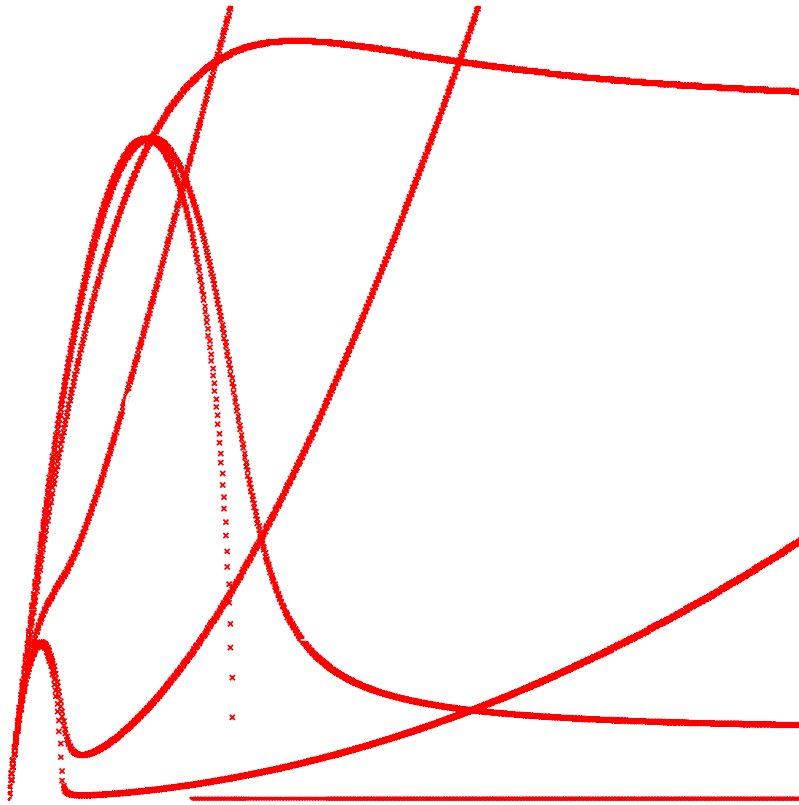
Fig. 6.— Adiabatic evolution of a pressure confined cloud engulfed by a wind moving at a Mach number $M = 0.8$; the density contrast is $D = 0.002$. Evolutionary times shown are (a) 0, (b) 1.32, (c) 2.43, (d) $3.53\tau_d$, where τ_d is the KHI characteristic time scale defined in Sec. 3. Contours correspond to logarithmic density levels and arrows show velocity field. The thick line in (d) represents the contour containing 90% of the initial cloud mass. The minimum and maximum densities (in units of the wind density) present are (a) 1-500, (b) 0.46-673, (c) 0.49-965 and (d) 0.4-514. The velocity range (in units of the isothermal sound speed in the wind) are (a) 0-1.03, (b) 0.001-1.86, (c) 0.005-1.86 and (d) 0.007-1.89. The grid is rectangular and cylindrical symmetry is assumed.

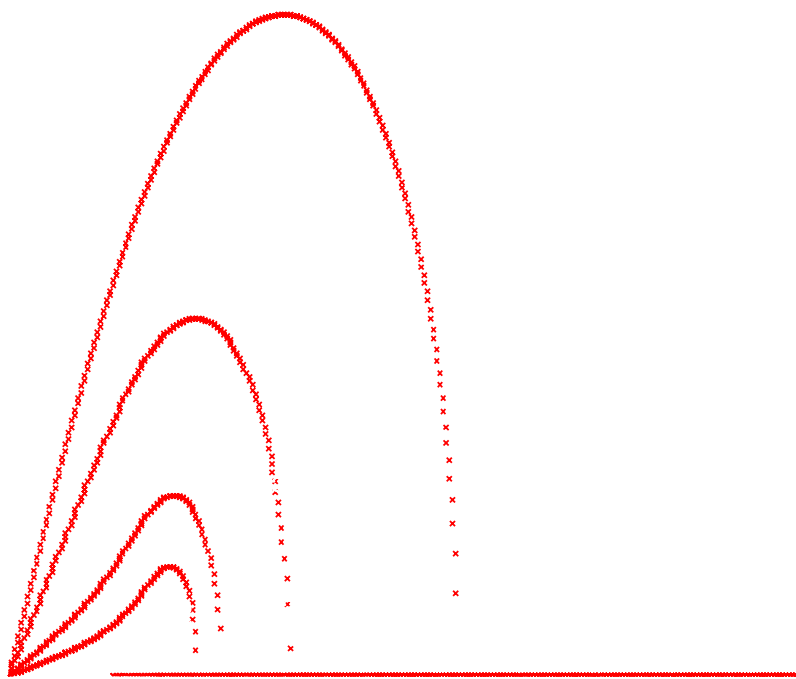
Fig. 7.— Radiative evolution of a pressure confined cloud engulfed by a wind moving at a Mach number $M = 0.8$. Evolutionary times shown are (a) 0, (b) 1.27, (c) 2.44, (d) $3.65\tau_d$, where τ_d is the KHI characteristic time scale defined in Sec. 3. Contours correspond to logarithmic density levels and arrows show velocity field. The thick line in (d) represents the contour containing 90% of the initial cloud mass. The minimum and maximum densities (in units of the wind density) present are (a) 1-500, (b) 0.6-1139, (c) 0.53-1066 and (d) 0.64-2053. The velocity range (in units of the isothermal sound speed in the wind) are (a) 0-1.03, (b) 0.001-1.55, (c) 0.0007-1.61 and (d) 0.002-1.53. The grid is rectangular and cylindrical symmetry is assumed.

Fig. 8.— Time evolution of the fractional volumes occupied by the innermost 25%, 50%, 75% and 90% of the initial mass, for both the adiabatic (open squares) and the radiative (open stars) cases shown in Fig. 7

Fig. 9.— Same as Fig. 7 but for later evolutionary times: (a) 4.47, (b) 5.28, (c) 6.44, (d) $7.47\tau_d$

Fig. 10.— Isobaric contours corresponding to the same case as shown in Fig. 7





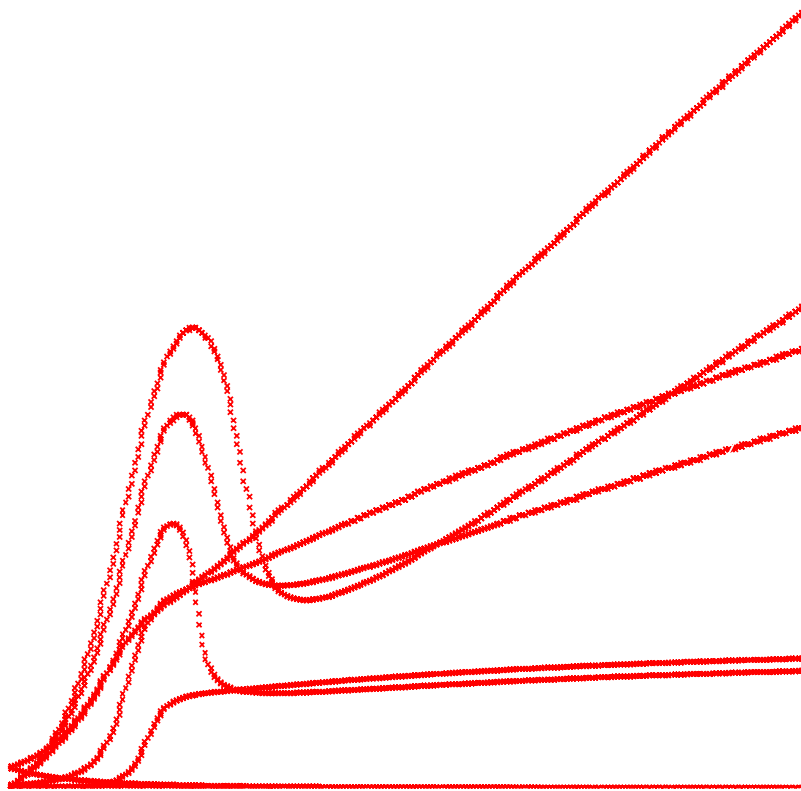
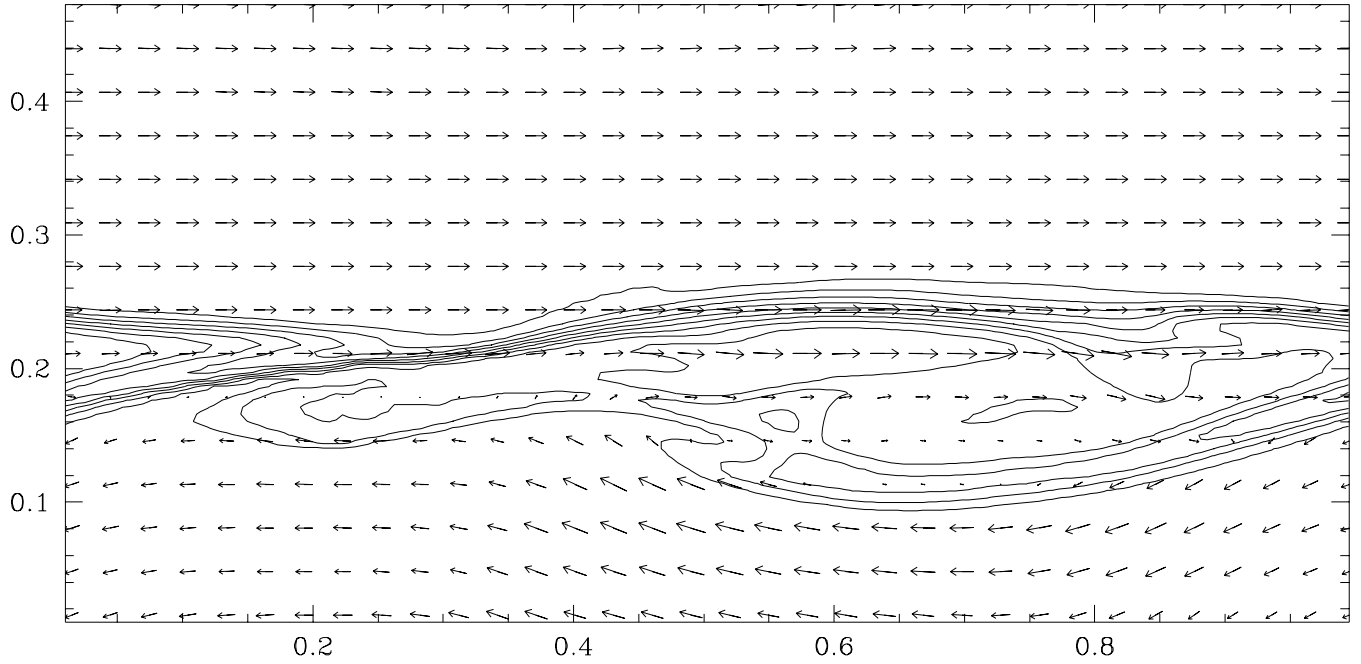
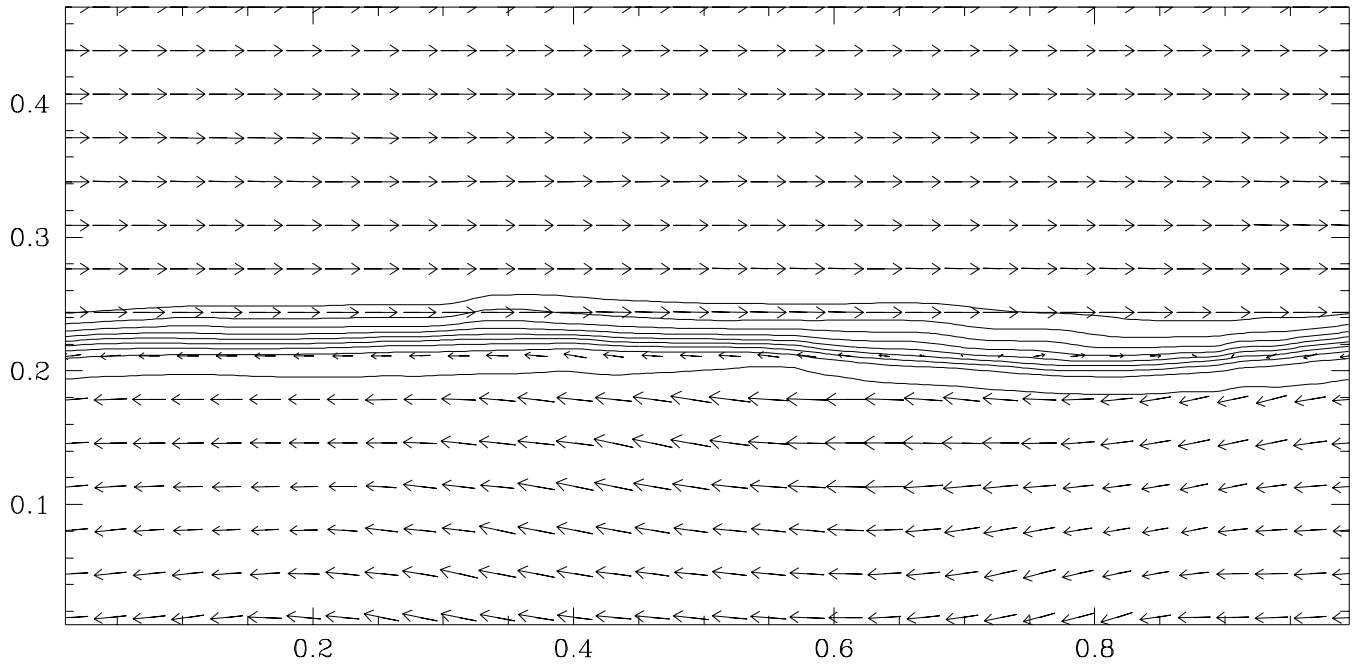


Fig. 4

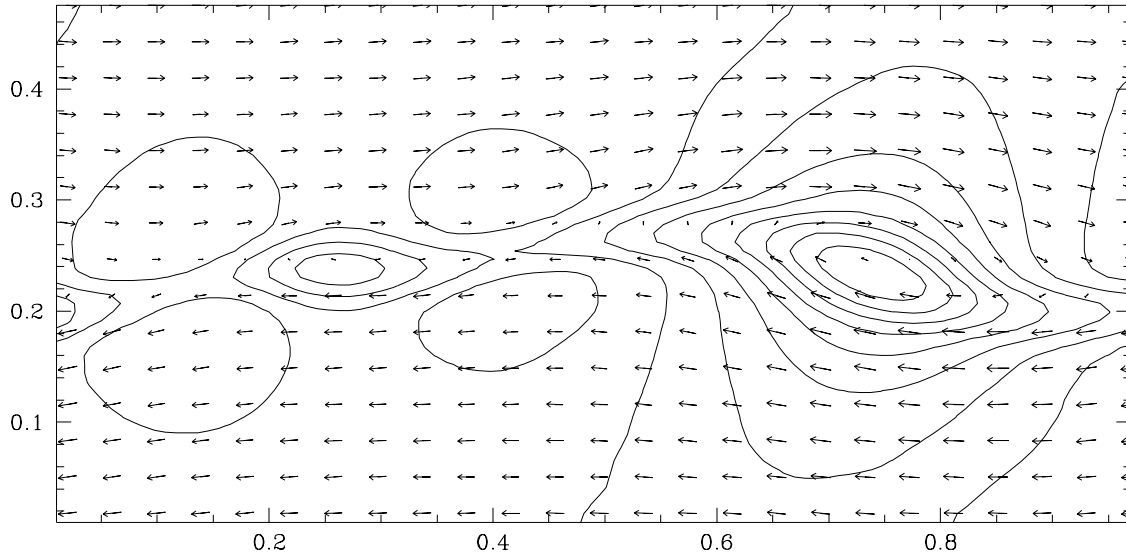


(a)

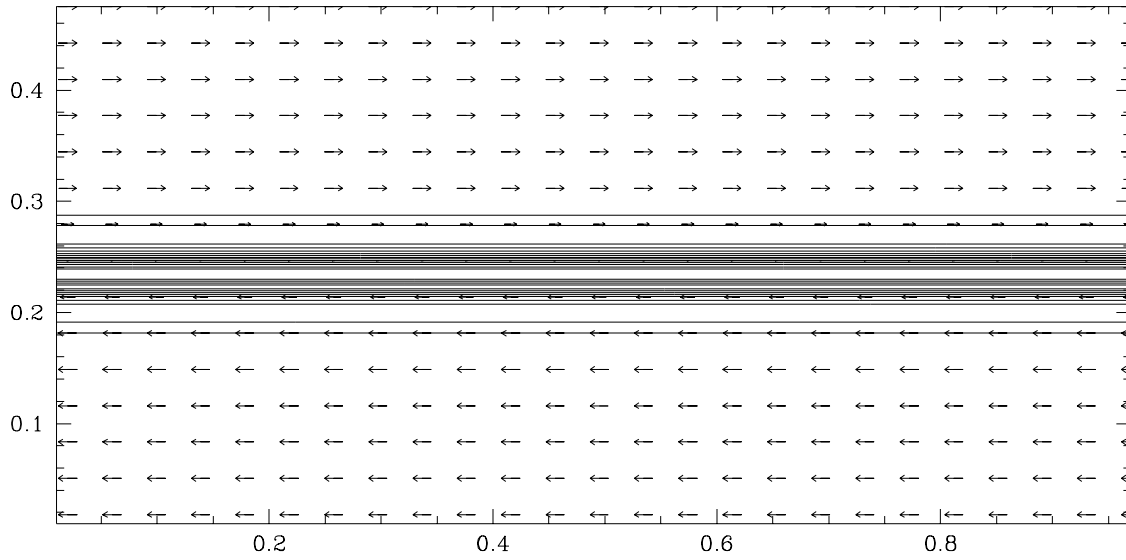


(b)

Fig. 5



(a)



(b)

Fig. 6

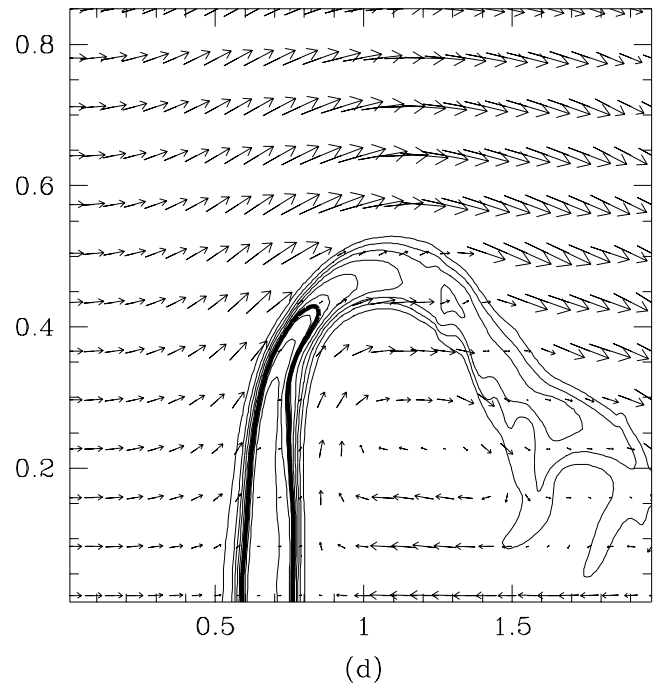
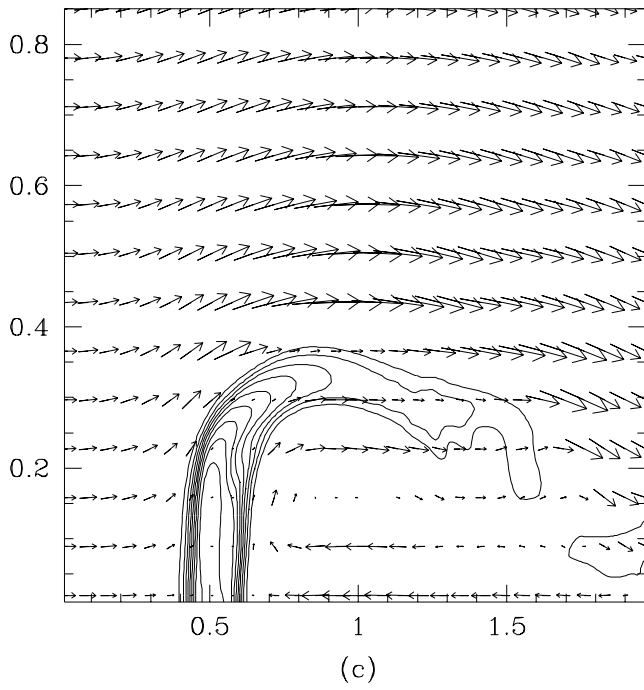
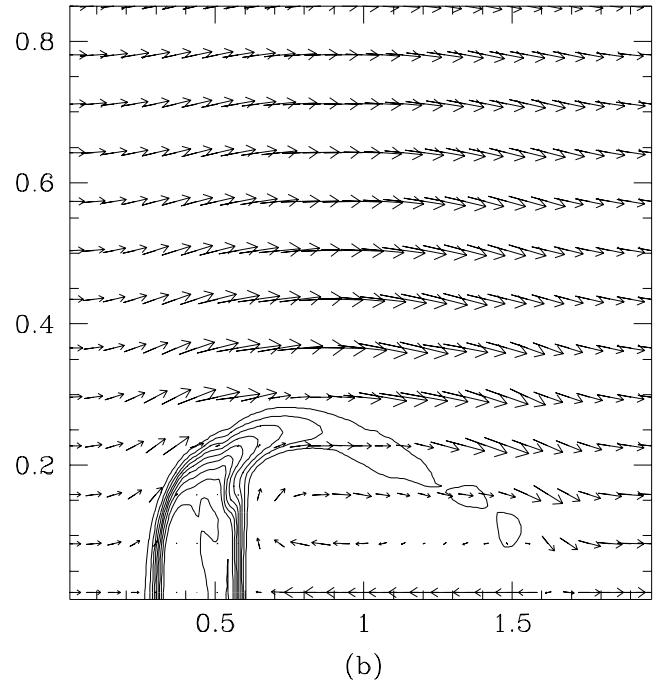
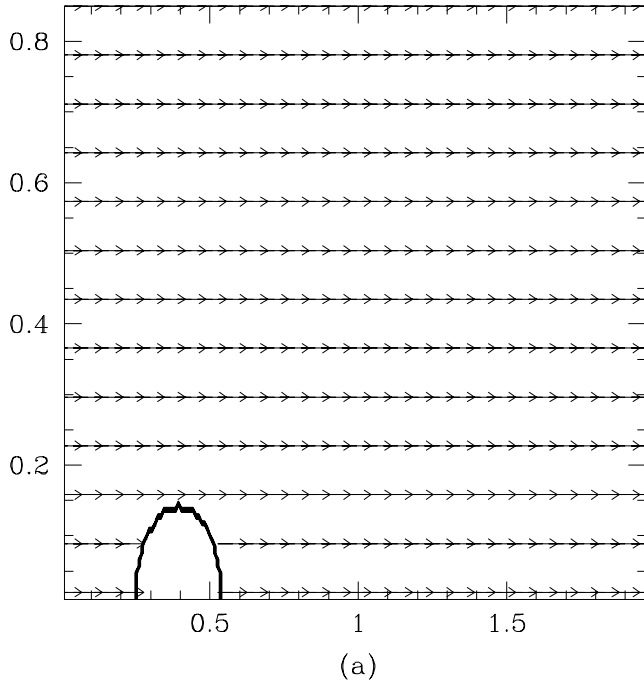


Fig. 7

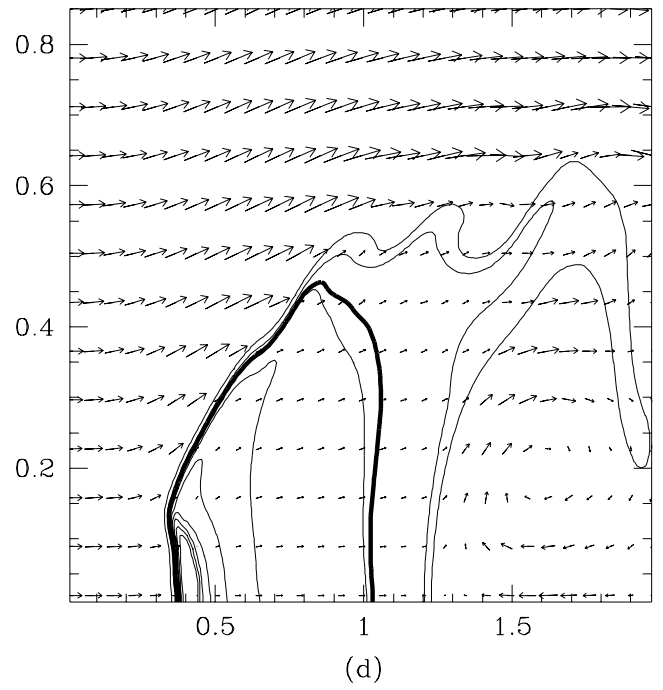
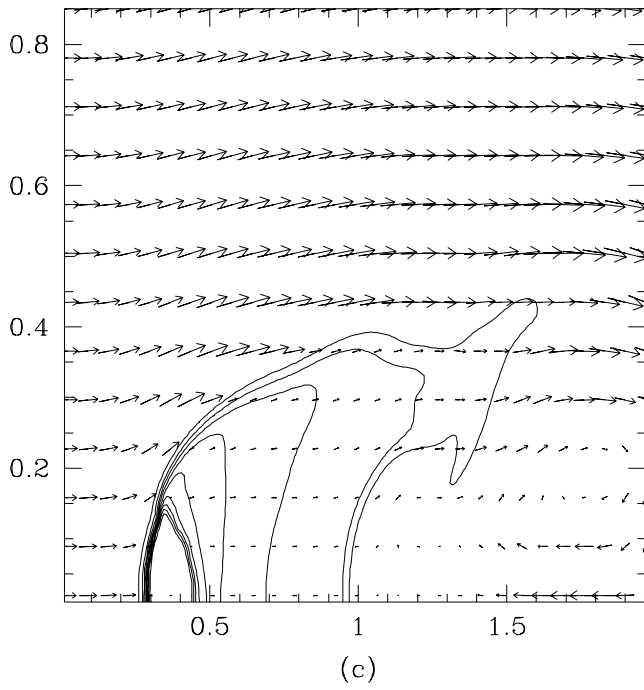
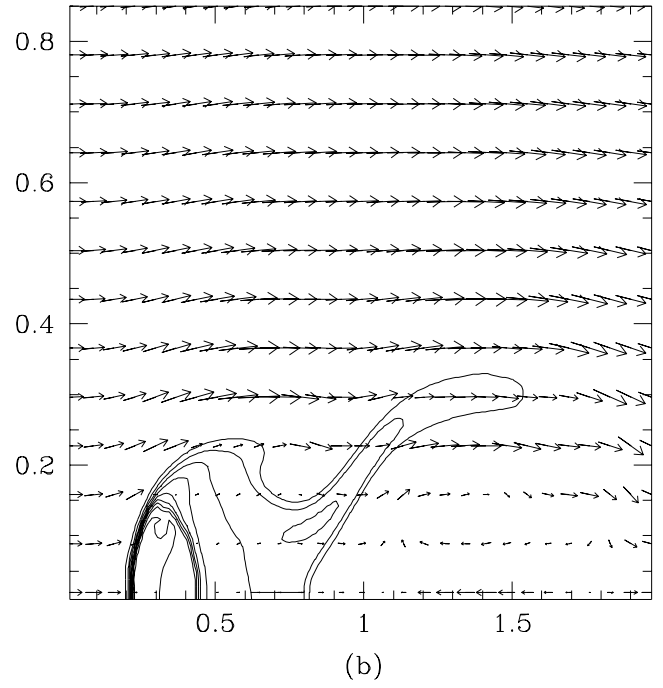
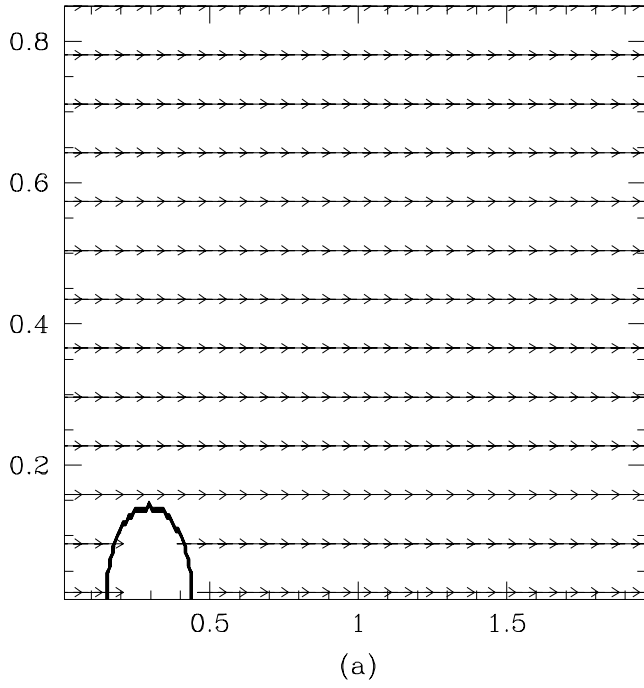


Fig. 8

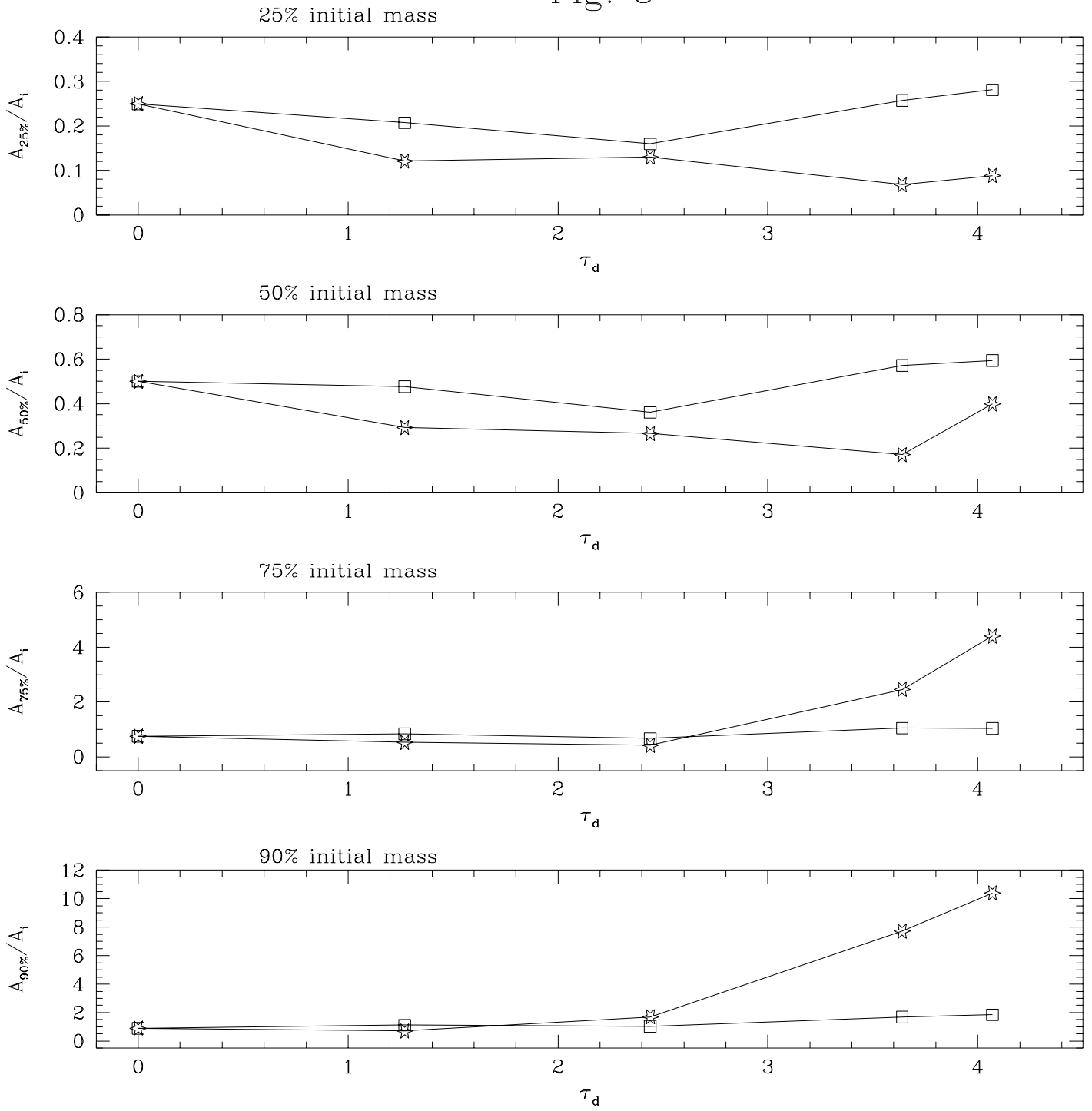


Fig. 9

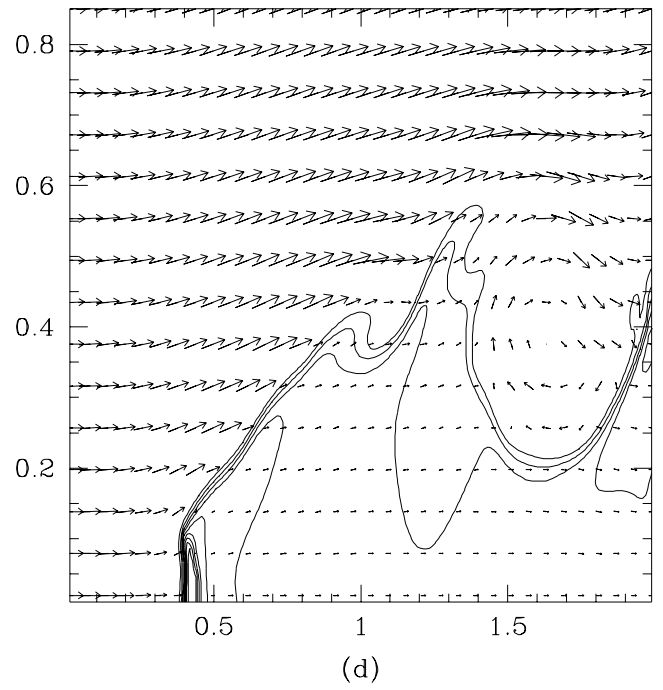
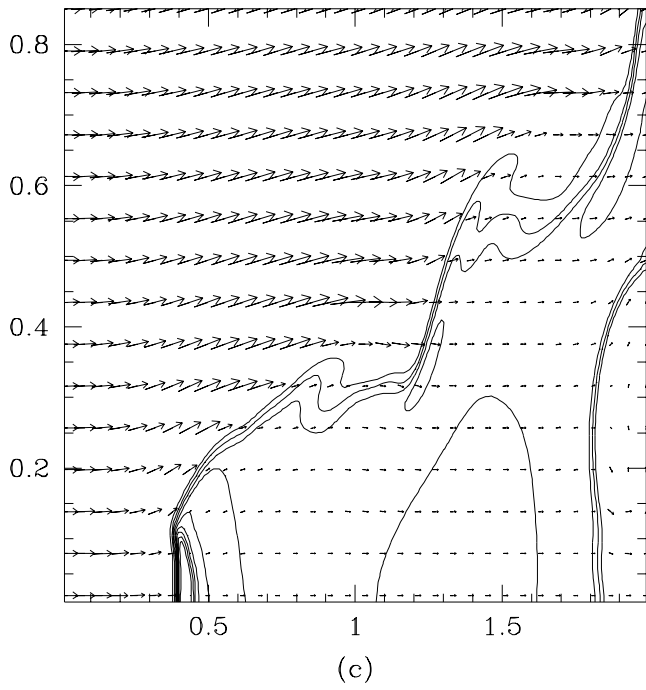
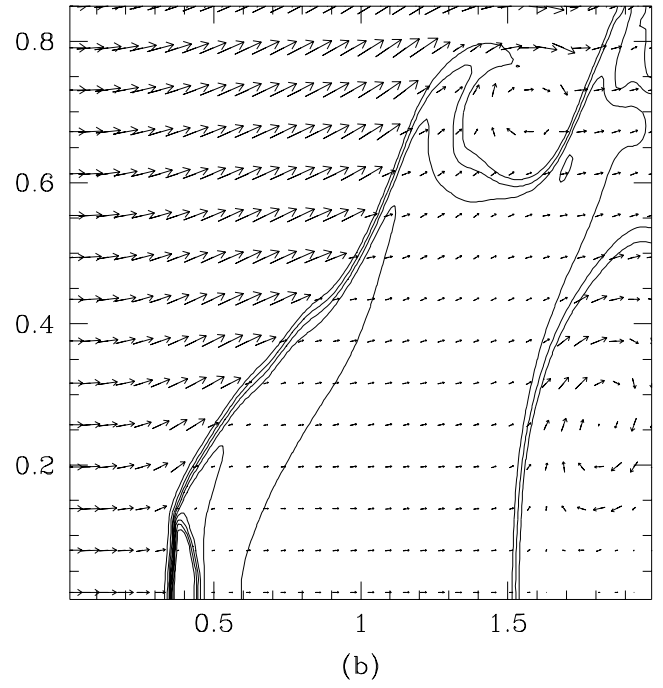
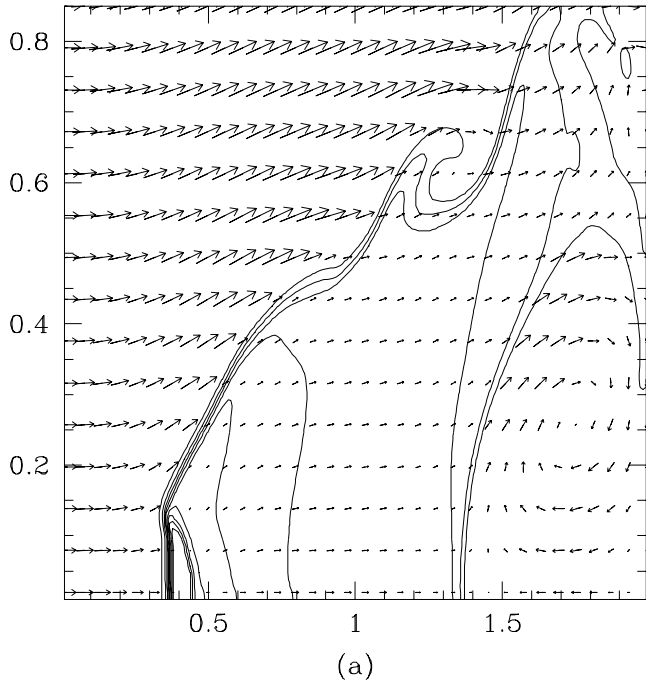
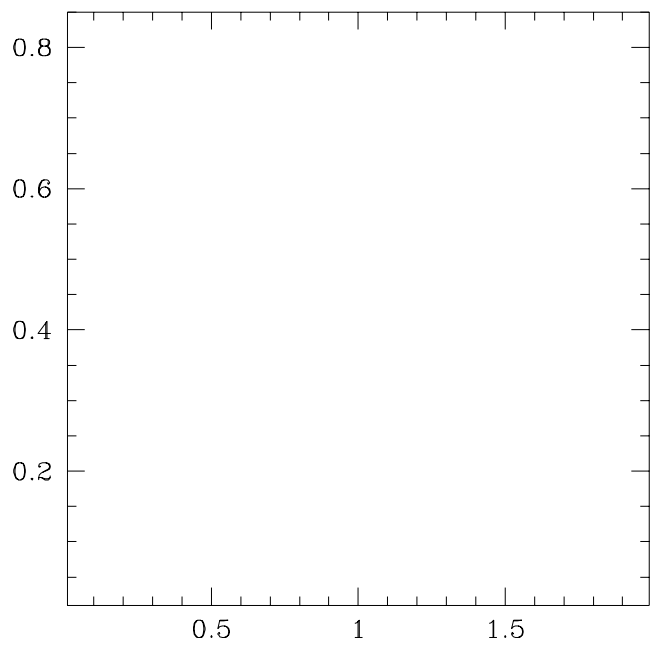
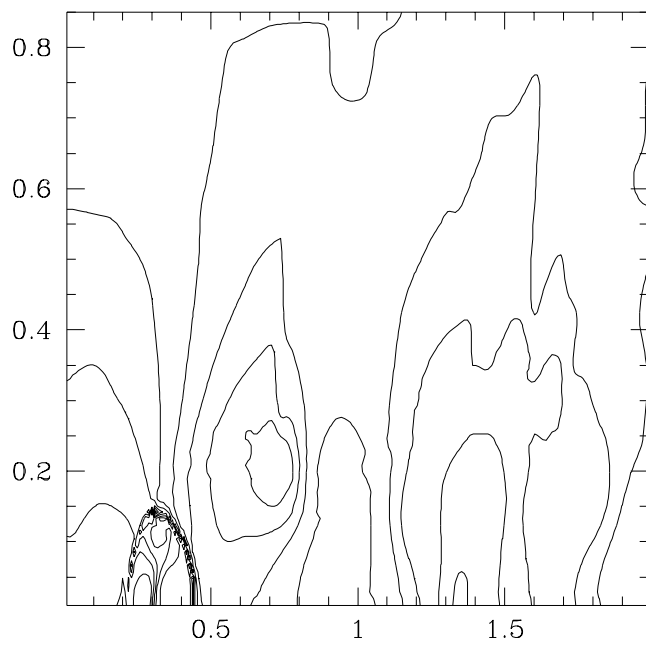


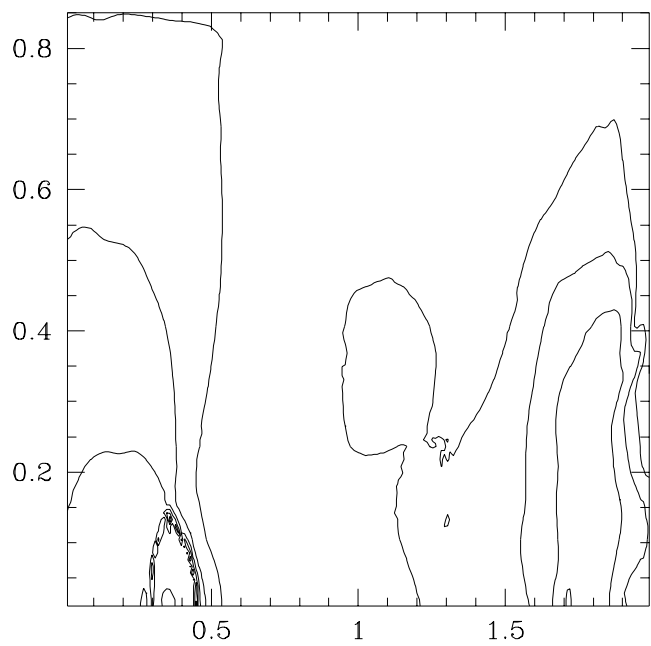
Fig. 10



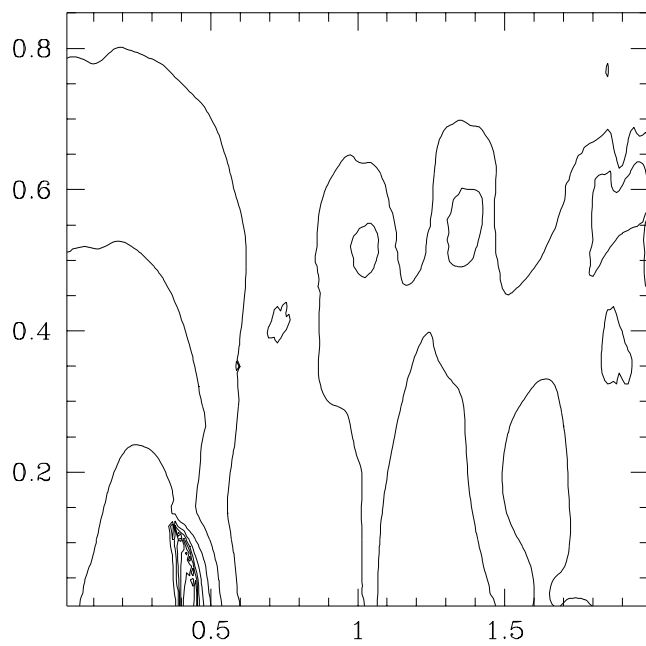
(a)



(b)



(c)



(d)